ELSEVIER

Seminars in
ULTRASOUND
CT and MRI

Pediatric Emergencies: Imaging of Pediatric Head Trauma

William T. O'Brien Sr., DO, Marguerite M. Caré, MD, and James L. Leach, MD

Pediatric head trauma is an important cause of morbidity and mortality in children and may be seen in the setting of accidental or abusive injuries. Although many of the patterns of head injury are similar to adults, the imaging manifestations of head injury in children are more complex due to the developing brain and calvarium. Additionally, there are unique considerations for mechanisms of injury in children, to include abusive head trauma and birth-related injuries. The primary role of the radiologist is to identify and characterize the type and severity of head injury to help guide appropriate patient management.

Introduction

Pediatric head injuries are exceedingly common and may be seen in both the emergency and outpatient clinical settings. Regarding accidental injuries, motor vehicle accidents involve all age groups but occur more frequently in older children and adolescents. In younger children, falls are more prevalent, whereas bicycle and sports-related injuries are more common in older children. Although many of the patterns of head injury are similar to adults, the imaging manifestations of head injury in children are more complex due to the developing brain and calvarium. Additionally, abusive head trauma and birth-related injuries are unique mechanisms of injury to be considered in the pediatric population. The primary role of the radiologist is to identify and characterize the type and severity of head injury to help guide appropriate patient management. This review article discusses important imaging findings and patterns of pediatric head injury with a focus on how head trauma in children differs from that seen in adults (Table). Topics covered include calvarial fractures, extra-axial hemorrhage, cortical contusions, diffuse axonal injury, abusive head trauma, and birth-related injuries.

Department of Radiology, University of Cincinnati College of Medicine, Cincinnati, OH.
Address reprint requests to William T. O'Brien, Sr., DO, Department of Radiology, University of Cincinnati College of Medicine, Cincinnati, OH. E-mail: William.obrien@cchmc.org

Imaging of Head Trauma in Children

As children are more sensitive and susceptible to the potential adverse effects of ionizing radiation, there is a greater focus on the appropriate usage of radiographs and computed tomography (CT) in the setting of pediatric head trauma. Ultimately, however, the risks of radiation have to be weighed against the need to identify clinically significant and treatable head injuries. With acute moderate to severe head trauma, acute head injury with altered mental status or neurological deficits, or in cases where symptomatic abusive head trauma is suspected, CT is warranted to identify intracranial injuries that may require immediate treatment.[1] In these settings, the lowest dose reasonable to attain the necessary diagnostic information should be used. Magnetic resonance imaging (MRI) may be appropriate as a follow-up study to identify additional or more subtle injuries that are not identified on CT and are important for patient management and prognosis. In patients with minor head injury, no loss of consciousness or neurological deficits, and no clinical findings suggesting significant head injury, imaging in the acute setting may potentially be avoided.[2] In patients with a subacute injury and delayed clinical presentation, MRI is preferred to CT.[1]

Calvarial Fractures

Although the pediatric skeleton tends to be more pliable and resistant to fractures compared to adults, calvarial fractures are

https://doi.org/10.1053/j.sult.2018.01.007

Table Key Imaging and Clinical Features Specific to Pediatric Head Trauma

Calvarial fractures
3-D postprocessing helps distinguish fractures from sutures
Sutures have "zig-zag" course; fractures are linear
Sutures merge; fractures may cross or widen sutures
"Ping pong" fractures may be seen in kids due to malleable bones
Intracranial hemorrhage
Fractures are less often seen with EDHs in kids compared to adults
Cortical contusions are less frequent and may occur in atypical locations in kids
Abusive head trauma
SDH (especially mixed density) with incompatible trauma history is suspect for AHT
Internal septations in SDHs suggest chronicity
One should be cautious in attempting to date SDHs
Stellate fractures are more common in AHT than accidental trauma
Bridging vein injury in the absence of appropriate trauma history is suspect for AHT
Hypoxic-ischemic injury is more common in AHT than accidental trauma
Birth-related injuries
Small SDHs are commonly seen in normal birthing process incidentally
Calvarial fractures and molding may occur during birthing process
Cephalohematomas are subperiosteal and do not cross the sagittal suture
Caput succedaneum and subgaleal hematomas may cross sutures

EDH, epidural hematoma; SDH, subdural hematoma.

not uncommon in children with head trauma, especially in infants who have limited trabecular maturation and structural support. Identifying calvarial fractures in children can be challenging due to the presence of multiple primary and accessory sutures that may complicate identification of non-depressed fractures. However, there are imaging features that are helpful in distinguishing fractures from sutures, particularly in the acute setting.

Sutures occur in predictable locations and the paired primary sutures are symmetric. The primary sutures include the midline sagittal suture between the parietal bones, paired coronal sutures located between the frontal and parietal bones, paired lambdoid sutures between the parietal and occipital bones (continuous with the occipitomastoid sutures inferiorly), and the midline metopic suture between the frontal bones. The squamosal suture extends from the pterion (junction of the frontal, parietal, temporal, and sphenoid bones) anteriorly to the junction of the lambdoid and occipitomastoid sutures posteriorly. The anterior fontanelle is situated between the sagittal and coronal sutures, and the smaller posterior fontanelle is situated between the sagittal and lambdoid sutures (Fig. 1). Accessory sutures occur most frequently in the occipital and parietal bones due to the increased number of ossification centers. The occipital bone typically forms from 6 ossification centers, 4 centered around the foramen magnum and 2 for the posterior squama. The parietal bones typically form from 2 ossification centers.[3,4] Accessory sutures may be bilateral and symmetric or unilateral.[5] When unilateral, evaluation for symmetry becomes unreliable in excluding a fracture.

In the acute setting, fractures present as lucent, cortical defects that lack sclerotic borders, whereas sutures often (but not always) have sclerotic margins. For orientation, fractures

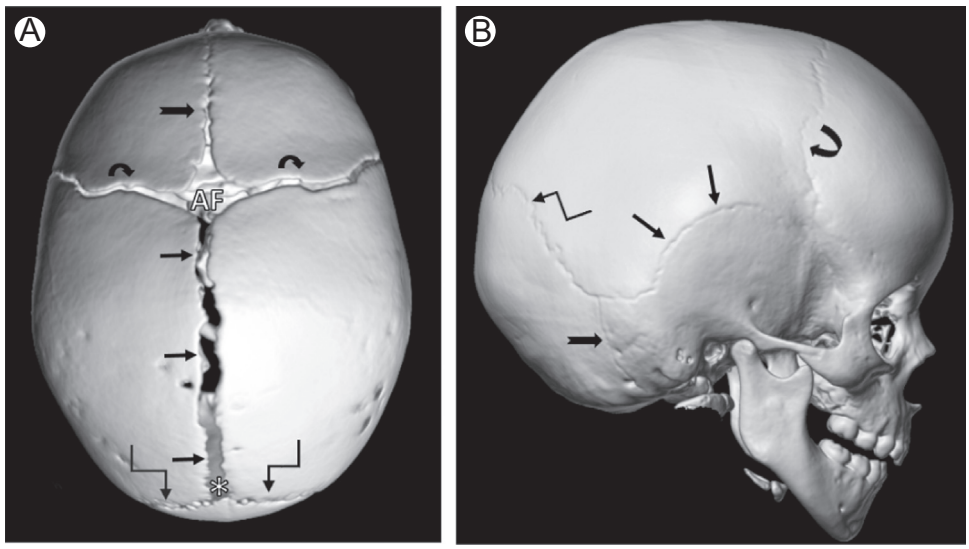

Figure 1 Normal sutures and fontanelles. Volume rendered (VR) image of the cranial vertex in a 2-month-old infant (A) depicts the anterior fontanelle (AF) at the junction of the sagittal (straight arrows), coronal (curved arrows), and patent metopic (notched arrow) sutures. The posterior fontanelle (*) is located at the junction of the sagittal (straight arrows) and lambdoid (elbowed arrows) sutures. Lateral VR projection in a 4-year-old child (B) shows the squamosal suture (straight arrows) extending from the coronal suture (curved arrow) anteriorly to the junction of the lambdoid (elbowed arrow) and occipitomastoid (notched arrow) sutures posteriorly.

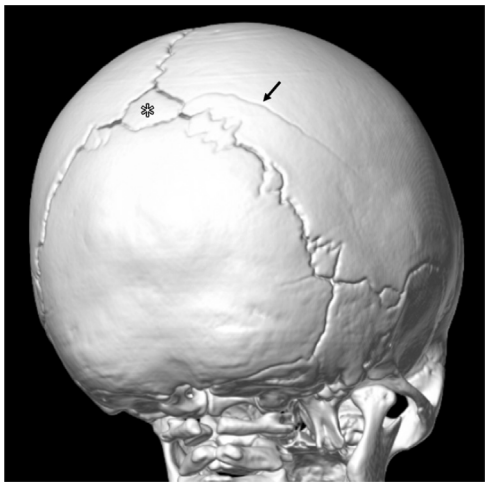

Figure 2 Fracture vs suture orientation. VR image from a posterior oblique projection shows a linear left posterior parietal bone fracture (black arrow) extending inferiorly from the preinterparietal Wormian (inca) bone (*) at the junction of the sagittal and lambdoid sutures. The fracture has a linear orientation as opposed to the "zig-zag" orientation of the visualized sutures.

tend to be linear, whereas sutures have a characteristic "zig-zag" course (Fig. 2). Sutures merge with one another as they coalesce, whereas fractures may cross over or extend into and widen sutures, which is referred to as sutural diastasis (Fig. 3).

Depressed fractures are readily identified on imaging due to the inward displacement of the calvarium at the site of impact (Fig. 4). It is important to annotate the depth of depression for management and prognosis. In general, the greater the depression, the higher the likelihood of underlying intracranial injuries. As the pediatric skull is more malleable than adults, especially in newborns and infants, a focal calvarial depression may occasionally occur, often without a fracture lucency. This type of injury is referred to as a "ping pong" fracture, since it simulates a dented ping pong ball (Fig. 5).[6]

A leptomeningeal cyst refers to a "growing" fracture that is unique to children and occurs most frequently in patients under 3 years of age. It is thought to result from pulsations of cerebrospinal fluid (CSF) extending into and expanding the fracture. Leptomeningeal cysts are uncommon, occurring in less than 1% of calvarial fractures. CSF or a region of encephalomalacia extends through the calvarial defect on CT (Fig. 6).[7]

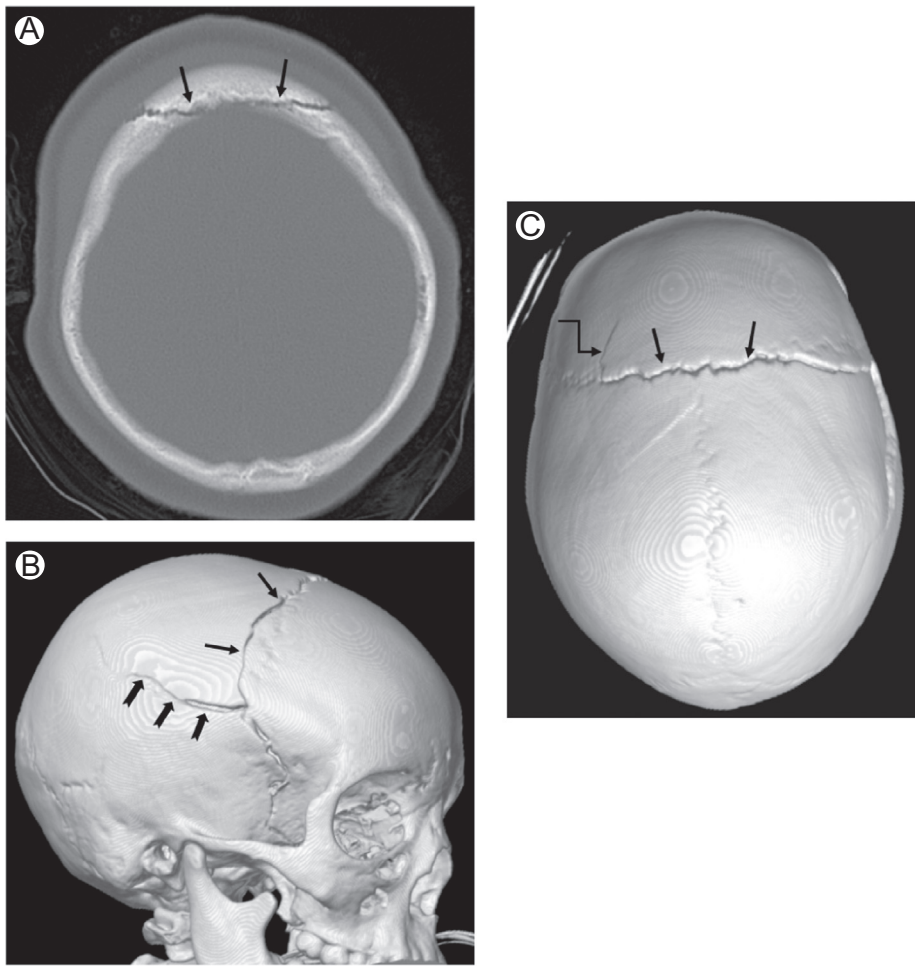

Figure 3 Sutural diastasis in a young child involved in a motor vehicle accident. Axial CT image in bone window (A) reveals abnormal widening of the coronal suture at the cranial vertex and extending bilaterally (black arrows). Lateral VR projection (B) shows a linear left parietal bone fracture (notched arrows) that extends into and widens the coronal suture (black arrows). VR image at the cranial vertex (C) shows the coronal suture diastasis crossing midline (black arrows) with an additional fracture component extending into the frontal bone on the right (elbowed arrow).

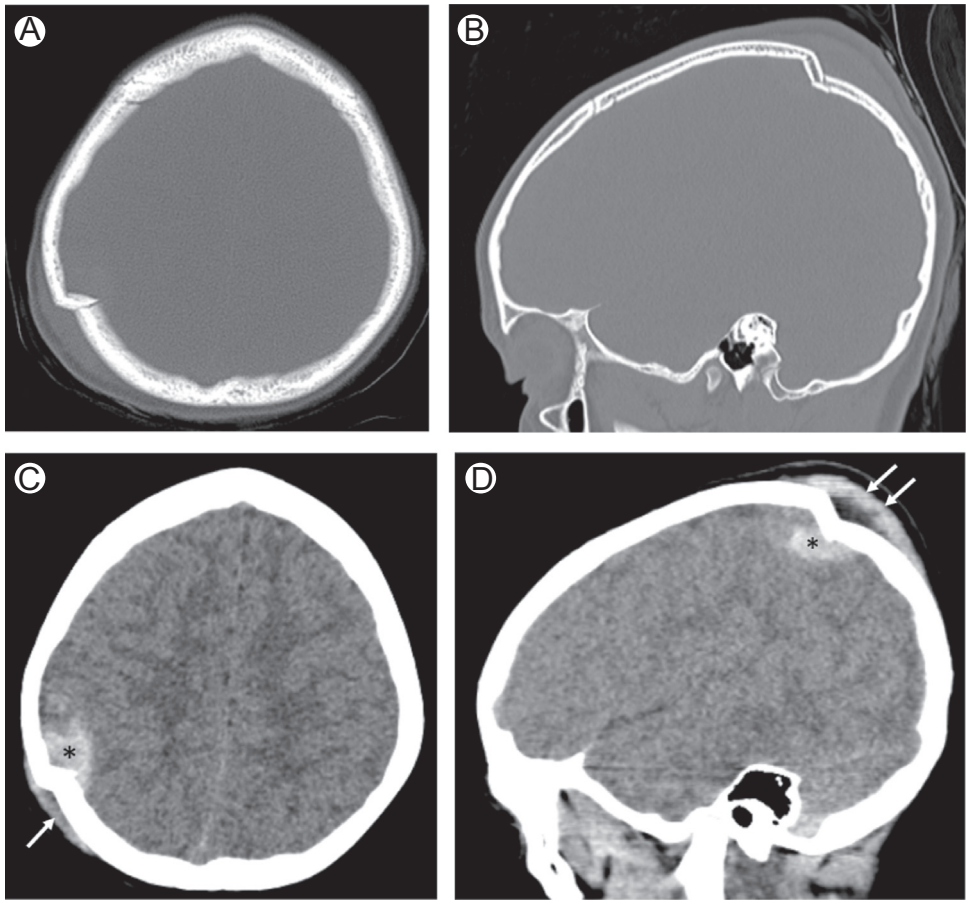

Figure 4 Depressed calvarial fracture with intracranial injuries. Axial (A) and sagittal reformatted (B) CT images in bone window show a comminuted depressed right parietal bone fracture with inward angulation. Corresponding images in brain window (C and D) show associated intracranial hemorrhage (*) and a superficial scalp hematoma (arrows).

On CT, fractures that are nondisplaced and oriented similar to the plane of imaging can easily be overlooked. For these reasons, it is important to review the scout image, have reformatted images available in at least 2 planes (commonly axial and coronal or all three planes in the setting of trauma), or use 3-dimensional reconstructions to appropriately evaluate the calvarium (Fig. 7).

Skull base fractures can be subtle and difficult to identify on imaging, especially in the presence of multiple accessory sutures. When fractures extend into pneumatized and aerated

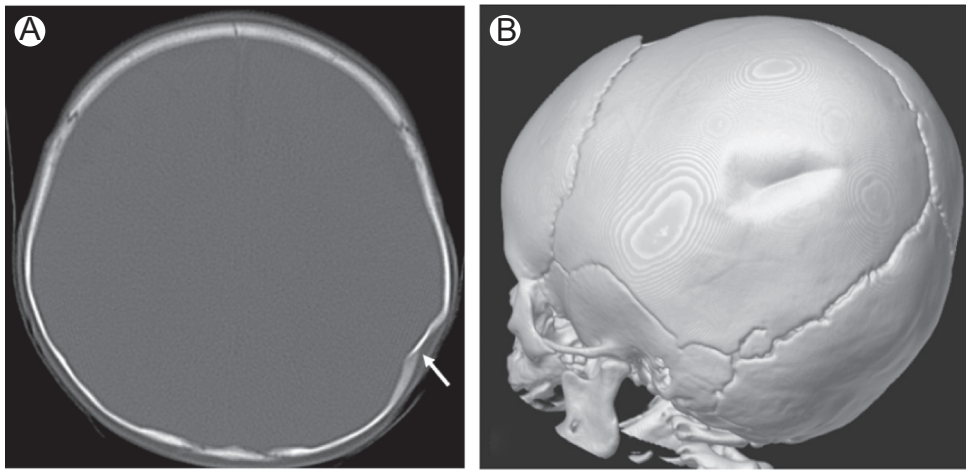

Figure 5 "Ping pong" fracture in an infant post-trauma. Axial CT image in bone window (A) reveals a focal depression involving the left parietal bone without a discernible fracture lucency (arrow). VR image in a lateral oblique projection (B) illustrates how the depression is similar to a dented ping pong ball.

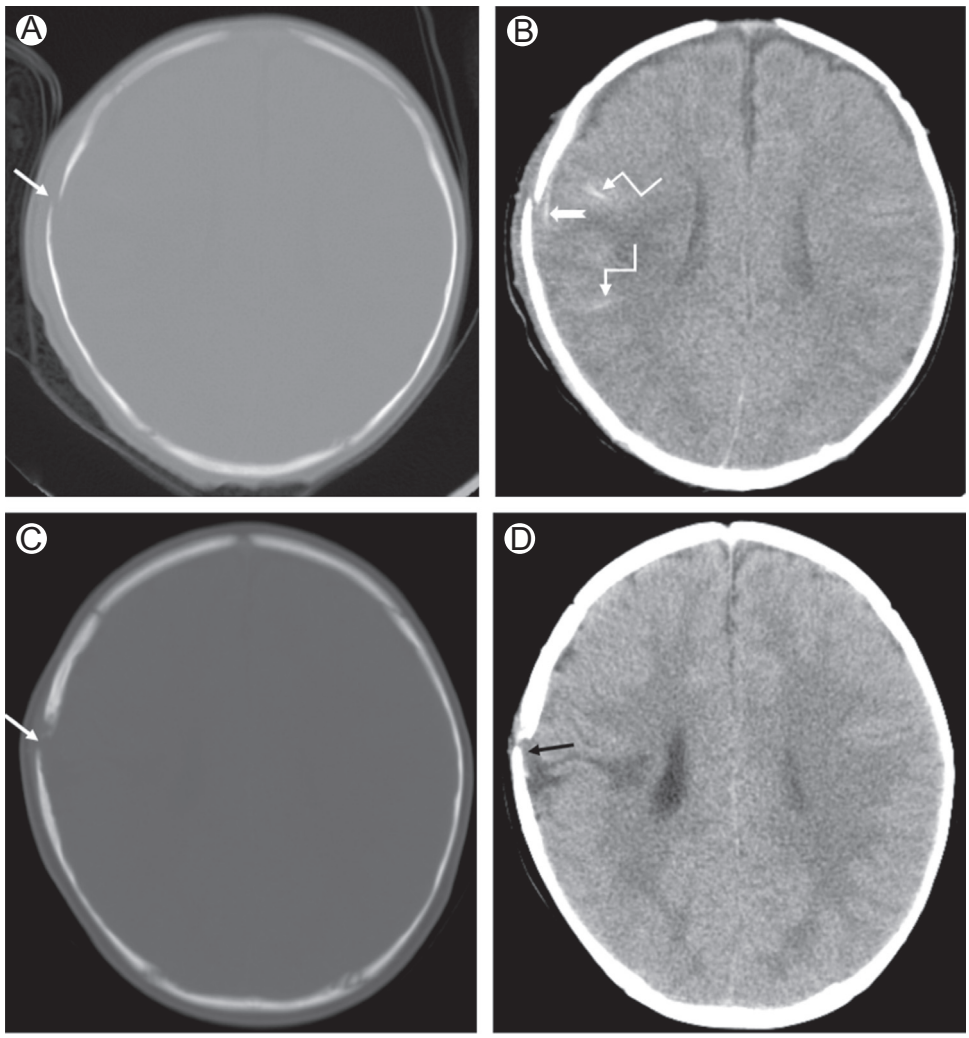

Figure 6 Leptomeningeal cyst ("growing" fracture) in a child after a motor vehicle accident. Axial CT image in bone window (A) shows a mildly displaced right parietal bone fracture (white arrow). Corresponding axial image in brain window (B) reveals underlying extra-axial (notched arrow) and subarachnoid (elbowed arrows) hemorrhage, as well as cortical contusions with surrounding edema. Follow-up CT image in bone window 6 months later (C) shows widening of the calvarial fracture (white arrow). Corresponding image in brain window (D) reveals cerebrospinal fluid extending into the fracture lucency (black arrow) with underlying encephalomalacia.

cavities, such as the paranasal sinuses, mastoid air cells, or middle ear cavities, secondary findings of layering hyperdense fluid (hemorrhage) within the aerated cavities should prompt closer evaluation for an underlying fracture (Fig. 8). Pneumocephalus may also be seen as the fracture leads to communication of the aerated cavity with the cranial vault. Anterior or central skull base fractures may have additional orbital or facial bone fractures. Central skull base fractures may involve the carotid canal, jugular foramen, or dural venous sinus channels, resulting in vascular injury or occlusion (Fig. 9).

Secondary findings commonly associated with calvarial fractures include superficial soft tissue swelling or underlying extra-axial hemorrhage, pneumocephalus, and parenchymal contusions. Diffuse axonal injury may also be seen. With delayed presentation, as may be seen in some cases of abusive head trauma, secondary findings may no longer be present at the time of imaging; therefore, their absence does not exclude prior trauma.

Extra-Axial Hemorrhage

Extra-axial hemorrhages are common in the setting of head trauma and are classified as epidural, subdural, or subarachnoid in location based upon the compartment in which they occur. At times, it may be difficult on imaging to distinguish between epidural and subdural hematomas, especially when small and not located in midline or along a suture.

In the acute setting, extra-axial hemorrhages are typically hyperdense compared to gray matter on CT. In the subacute stage, they become isodense to underlying gray matter, at which point they may be overlooked if not looking carefully at the peripheral cortical boundaries. In the chronic stage, extra-axial hemorrhage is hypodense to gray matter (Fig. 10). One imaging pitfall in the CT imaging appearance of an extra-axial hemorrhage occurs in the hyperacute stage where portions of the hemorrhage may appear isodense or even slightly hypodense compared to gray matter due to unclotted blood products.[8] The imaging appearance and typical evolution

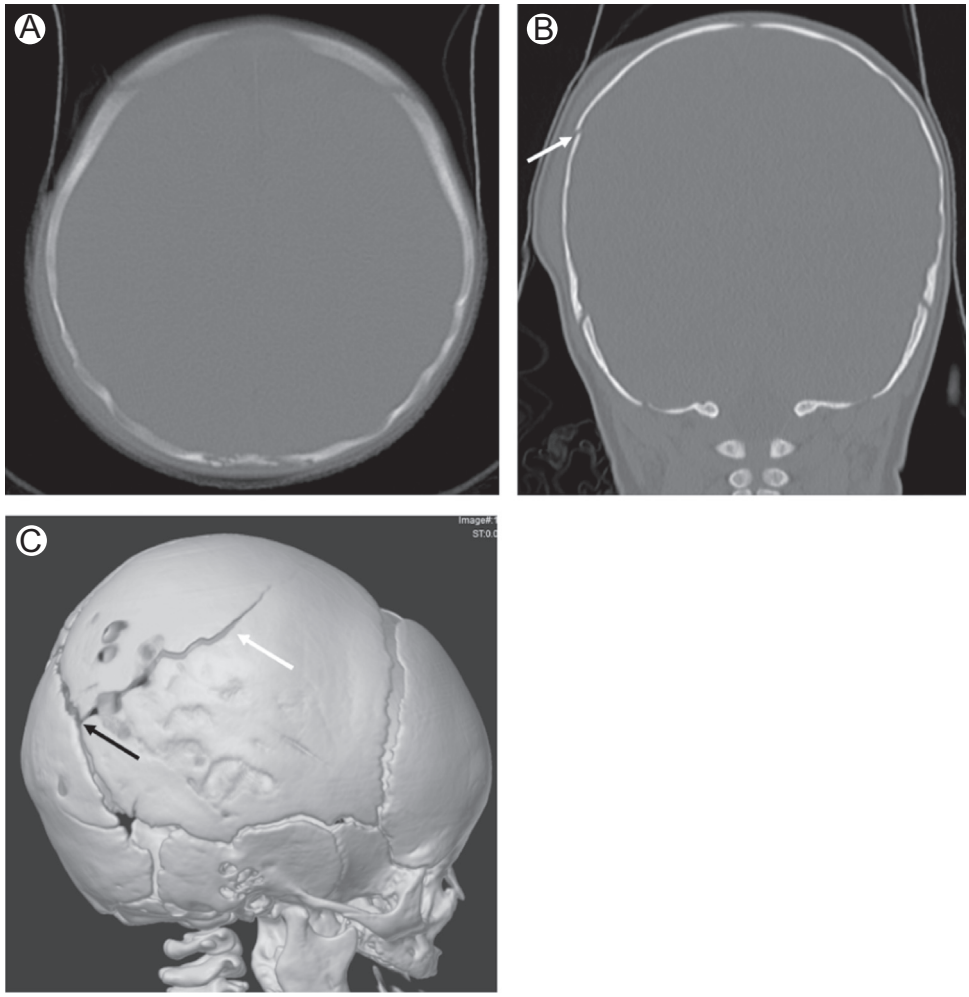

Figure 7 Subtlety of fractures in the plane of imaging. Axial CT image in bone window through the area of injury (A) reveals no discernible fracture. Corresponding image in the coronal plane (B) shows a minimally displaced right parietal bone fracture (arrow) with overlying scalp soft tissue swelling. VR image from a lateral projection (C) best depicts the extent of the fracture involving the mid to posterior portion of the parietal bone (white arrow) and extending to the lambdoid suture (black arrow).

pattern of hemorrhagic blood products may be altered with active hemorrhage, when there are hemorrhages of different ages, in patients with underlying anemia or coagulopathy, or with intermixing of CSF within the regions of hemorrhage.

Epidural Hematoma

The epidural space is located between the dura and overlying calvarium. The rigid dura extends into and firmly attaches to sutures; therefore, epidural processes are confined by and do not cross sutures (Fig. 11), with a few exceptions. Epidural hematomas result from tearing of epidural arteries (particularly the middle meningeal artery) or veins (increased incidence in children). They are characteristically lenticular or biconvex in shape (Fig. 12) and may cross midline. Although commonly associated with calvarial fractures in adults, epidural hematomas in children may occur in the absence of a calvarial fracture. Venous epidurals result from injury to dural venous sinuses; in this setting, the epidural hematoma may cross the sagittal suture or tentorium (Fig. 13). Injuries that result in disruption of the dura may also allow for an epidural hematoma to occasionally cross an overlying suture.

Most epidural hematomas are relatively uniform in density, although heterogeneous density is not uncommonly seen in the acute setting due to a combination of clotted (hyperdense) and unclotted (iso to hypodense) blood products. Although rare, an active bleed may be suggested when an enlarging hematoma demonstrates heterogeneous density with a swirling pattern (Fig. 14).[9] Epidural hematomas may require surgical evacuation due to mass effect or neurological decline.

Subdural Hematoma

The subdural space is a potential space located between the outer dura and inner arachnoid mater. Midline dural attachments define the subdural space. Therefore, subdural hematomas may extend along the outer margin of the cerebral hemispheres in a crescent shape, within the interhemispheric fissure, or layer along the tentorium (Fig. 15). Subdural processes may cross sutures but do not cross midline. Subdural

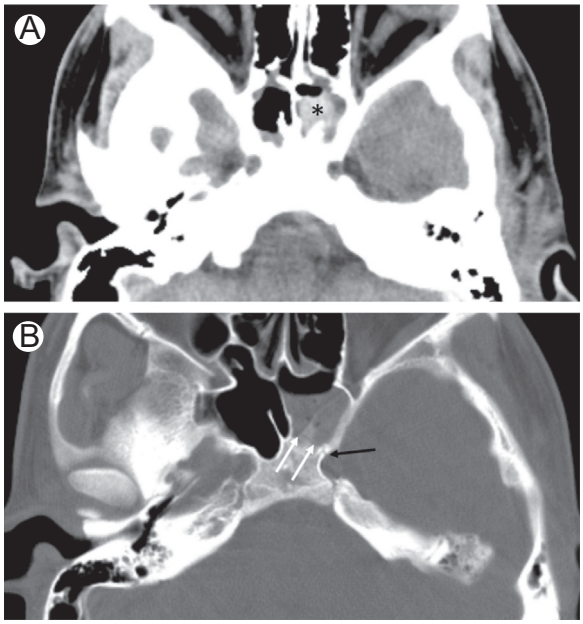

Figure 8 Hyperdense fluid within pneumatized spaces as a secondary finding of skull base fracture. Axial CT image in soft tissue window (A) demonstrates hyperdense fluid layering within the left sphenoid sinus (*), which prompted a second review of bone windows. Axial CT image in bone window (B), a few slices superior to image A, shows a subtle skull base fracture extending through the walls of the left sphenoid sinus (white arrows), as well as involvement of the carotid canal (black arrow).

hematomas result from injury to cortical bridging veins as they traverse the subdural space.

As discussed previously are typically hyperdense in the acute stage, isodense in the subacute stage, and hypodense in the chronic stage compared to underlying gray matter. The attenuation may be more heterogeneous due to intermixing of CSF within the subdural collections (hematohygroma) or in the setting of repeat or active hemorrhage (Fig. 16). Treatment often depends upon the size of the hematoma, degree of mass effect, and neurological status of the patient.

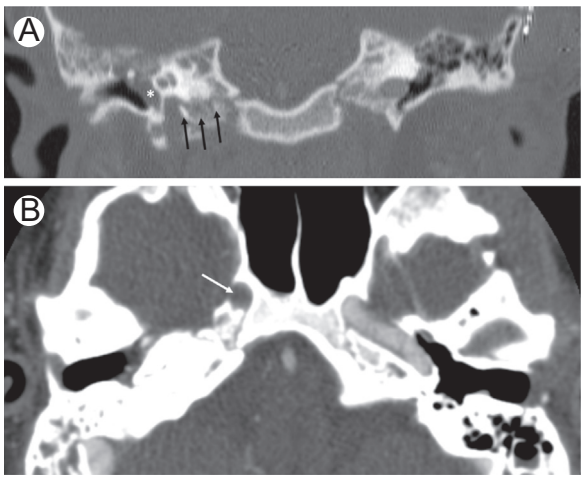

Figure 9 Vascular injury associated with skull base fractures. Reformatted coronal CT image in bone window (A) shows a skull base fracture on the right that involves the carotid canal (black arrows). There is complete opacification of the right middle ear cavity (*). Axial image from a follow-up CT angiogram (B) demonstrates absent contrast enhancement with occlusion of the distal petrous segment of the right internal carotid artery (white arrow).

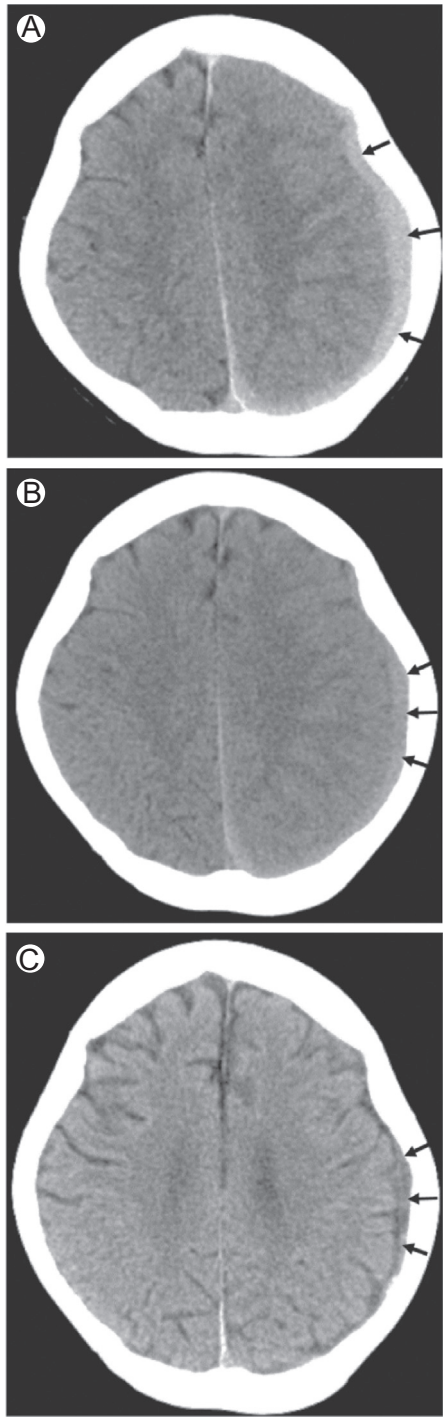

Figure 10 Stages of hemorrhage in a 14-year-old boy post-trauma. Initial axial noncontrast head CT image (A) shows a hyperdense subdural hemorrhage overlying the left cerebral convexity (arrows). On a follow-up study 1 week later (B), the hemorrhage is decreased in size and relatively isodense to underlying gray matter (arrows). Additional follow-up examination 1 month later (C) shows continued decrease in size of the subdural hemorrhage which is now hypodense compared to brain parenchyma (arrows).

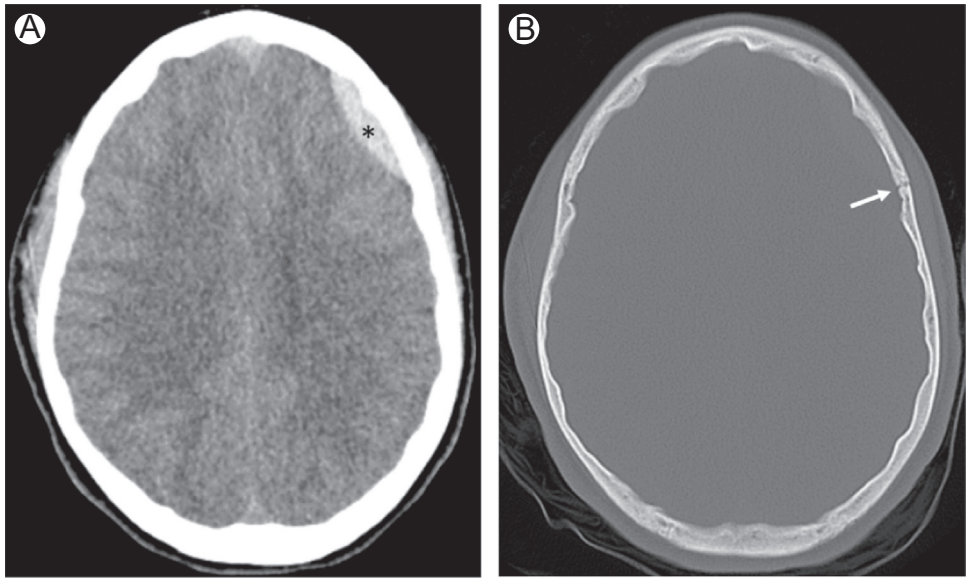

Figure 11 Epidural hemorrhage bounded by sutures. Axial noncontrast CT image in brain window (A) shows a hyperdense lenticular epidural hemorrhage overlying the left frontal lobe (*). Corresponding axial CT image in bone window (B) shows that the posterior margin of the hemorrhage in bounded by the coronal suture (arrow).

Subarachnoid Hemorrhage

The subarachnoid space is located between the overlying arachnoid mater and underlying pial covering of the brain parenchyma. Subarachnoid hemorrhage is common in the setting of head trauma, whereas a ruptured aneurysm represents the most common nontraumatic etiology of subarachnoid hemorrhage.

Subarachnoid hemorrhage appears as hyperdense foci typically located dependently within the cerebral sulci or CSF cisterns (Fig. 17). It is important to properly window and level each study to optimally evaluate for foci of hemorrhage. Commonly overlooked locations for subtle subarachnoid hemorrhage include the interpeduncular fossa and sylvian fissures.[10]

Pseudosubarachnoid Hemorrhage

In the setting of diffuse cerebral edema, relative hyperdensity within the basal cisterns may be noted in the absence of a true bleed (Fig. 18). This hyperdensity results from vascular engorgement secondary to increased intracranial pressures,

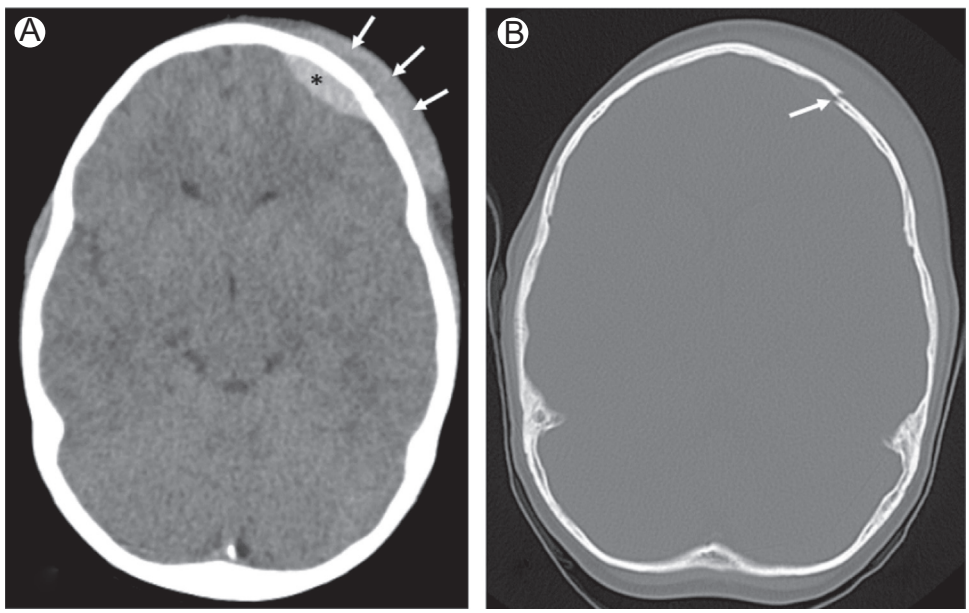

Figure 12 Epidural hemorrhage morphology. Axial noncontrast CT image in brain window (A) reveals a lenticular/biconvex hyperdense epidural hemorrhage (*) overlying the left frontal lobe. There is a prominent scalp hematoma (arrows). Corresponding CT image in bone window (B) shows a minimally displaced left frontal bone fracture (arrow).

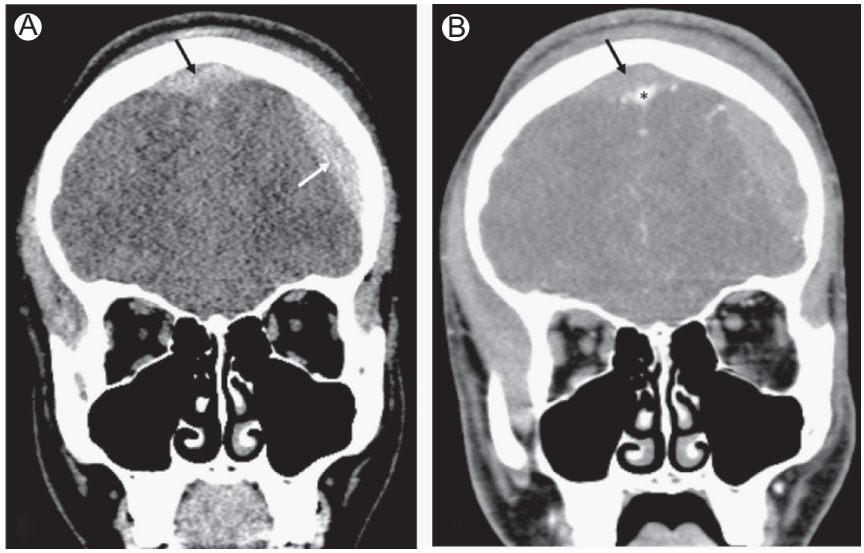

Figure 13 Venous epidural hemorrhage. Coronal reformatted CT image in brain window (A) demonstrates hyperdense extra-axial hemorrhage at the cranial vertex that crosses midline (black arrow). An acute left frontal extra-axial hemorrhage is also noted (white arrow). Coronal reformatted image from a follow-on CT venogram (B) shows that the cranial vertex hemorrhage (black arrow) is superficial to the contrast-opacified superior sagittal sinus (*), confirming its epidural location.

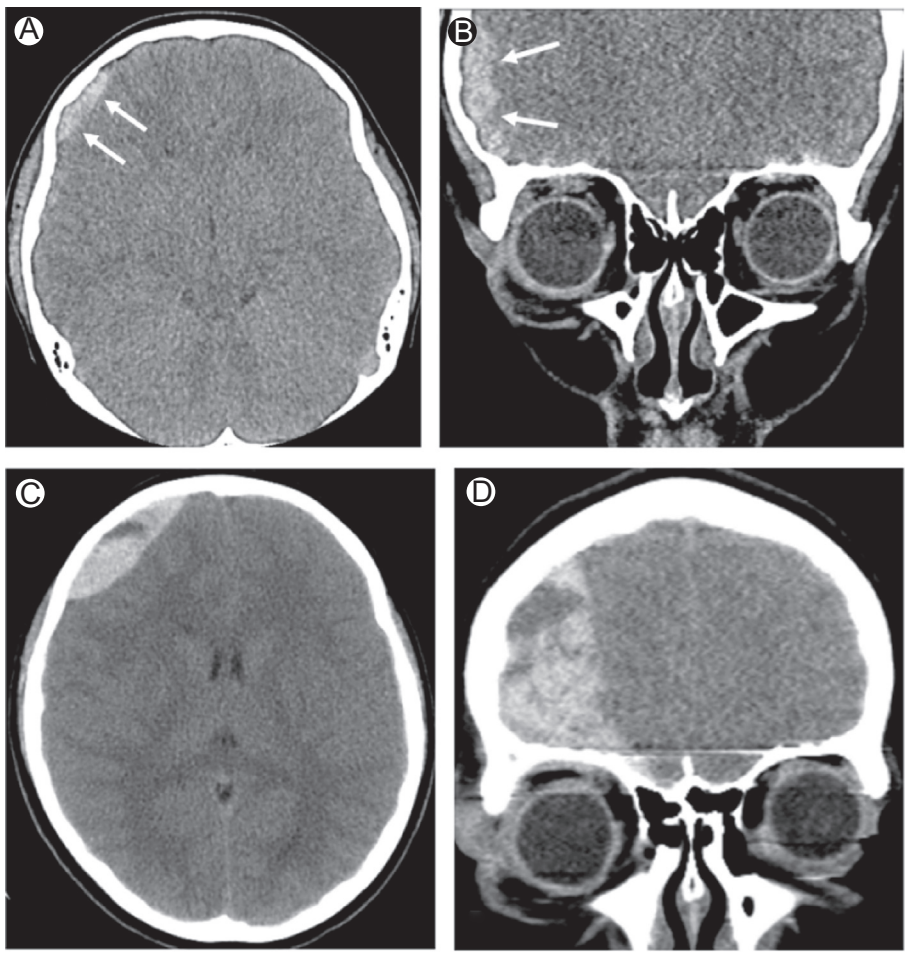

Figure 14 Active epidural hemorrhage with a swirling pattern. Axial (A) and coronal reformatted (CT) images from a facial CT performed at an outside facility following blunt trauma show a homogeneously hyperdense biconvex epidural hematoma overlying the right frontal lobe (arrows). Corresponding CT images from a noncontrast head CT performed 2 hours later due to acute clinical deterioration (C and D) demonstrate significant enlargement of the epidural hematoma, which has heterogeneous density with a swirling pattern, worrisome for active hemorrhage.

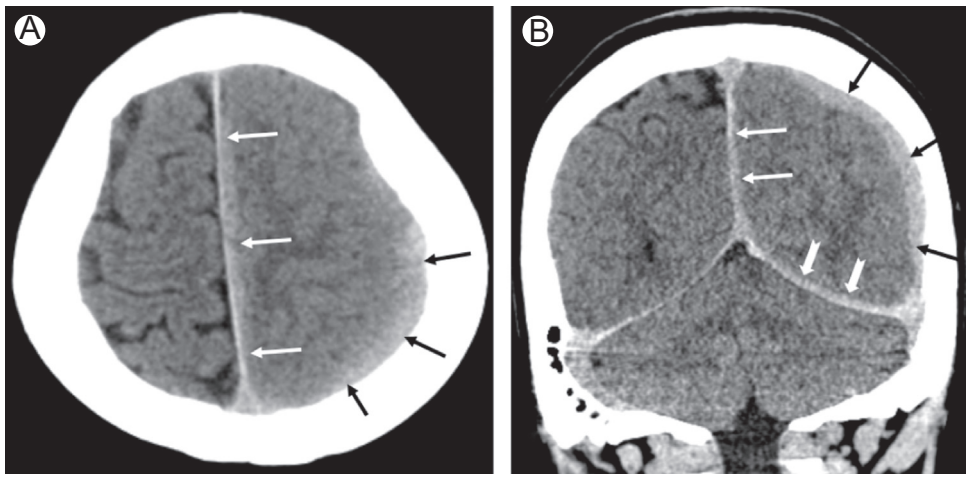

Figure 15 Subdural hemorrhage morphology and distribution. Axial noncontrast CT image in brain window (A) shows a hyperdense crescent-shaped subdural hemorrhage overlying the left cerebral hemisphere (black arrows) with extension along the interhemispheric fissure (white arrows). Coronal reformatted CT image in brain window (B) again demonstrates the subdural hemorrhage along the left cerebral convexity (black arrows) and interhemispheric fissure (white arrows), as well as subdural hemorrhage extending along the tentorium on the left (notched arrows).

along with effacement of CSF and cortical edema (hypodensity) within adjacent brain parenchyma. The attenuation associated with pseudosubarachnoid hemorrhage (30 Hounsfield units [HU]) is less than that of subarachnoid hemorrhage (55-70 HU).[11]

Cortical Contusions

Cortical contusions result from impact of the superficial brain parenchyma against a rigid surface, such as the inner margin of the calvarium or falx cerebri. Often times they occur at (coup) or opposite (contra-coup) the site of impact. Common locations include the inferior frontal lobes along the anterior cranial fossa, anteroinferior temporal lobes within the middle cranial fossae, and parasagittal locations adjacent to the falx. As the calvarium in children is less rigid than adults, cortical contusions occur less frequently in children and may occur in atypical locations.[12-14]

On CT, cortical contusions present as regions of hypodense edema or hyperdense foci of hemorrhage (Fig. 19). Extension into the subcortical white matter is not uncommon with larger contusions. Initially, these injuries may be subtle and become more conspicuous on short-term follow-up imaging over the next several hours or few days. As contusions may be multiple and occur bilaterally, care should be taken to identify additional regions of parenchymal injury. MRI has a greater sensitivity than CT in identifying cortical contusions (Fig. 20). When hemorrhagic, contusions will demonstrate foci of hemorrhagic susceptibility (hypointensity on T2* gradient echo [GRE] or susceptibility-weighted imaging

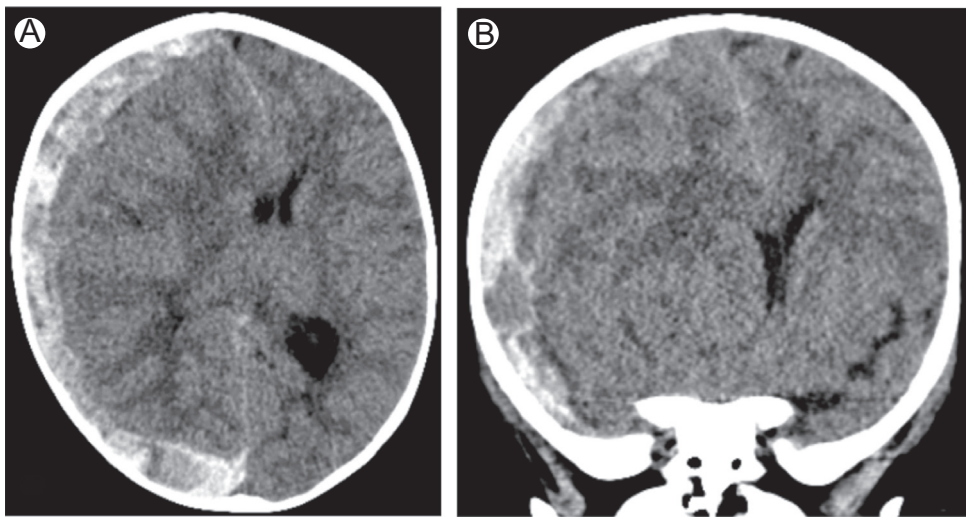

Figure 16 Heterogeneous subdural hemorrhage. Axial (A) and coronal reformatted (B) noncontrast CT images in brain window show a large mixed density subdural hemorrhage overlying the right cerebral convexity with marked mass effect, effacement of the right lateral ventricle, and midline shift with subfalcine herniation. The mixed density in this case is presumably attributed to a combination of unclotted hemorrhage and intermixing of cerebrospinal fluid.

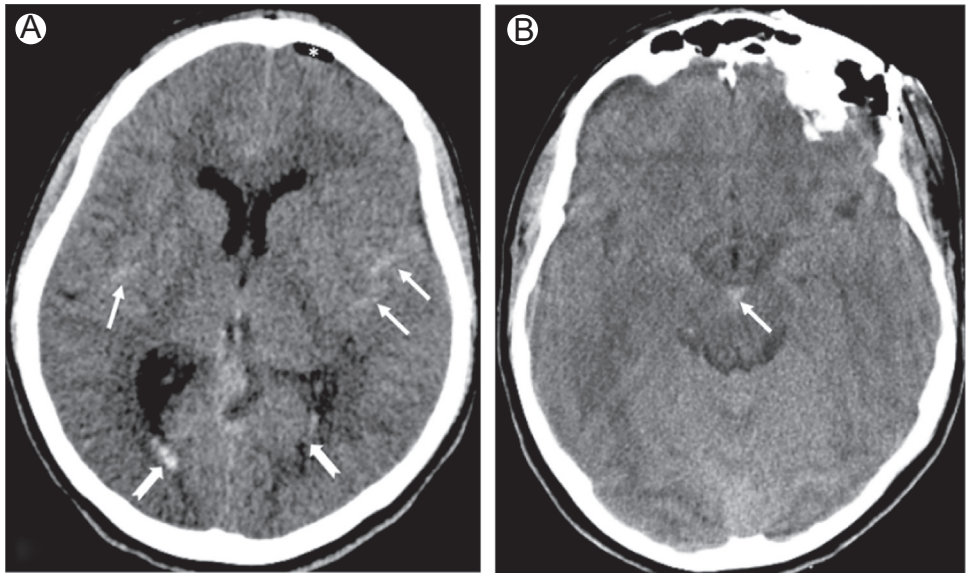

Figure 17 Subarachnoid hemorrhage following a motor vehicle accident. Axial noncontrast CT image through the level of the lateral ventricles (A) demonstrates hyperdense subarachnoid hemorrhage within the posterior aspect of the sylvian fissures (arrows) and within several sulci. A small amount of hemorrhage is seen within the occipital horn of the both lateral ventricles (notched arrows). There is a small focus of pneumocephalus overlying the left frontal lobe (*). Axial noncontrast CT image at the level of the basal cisterns (B) reveals a small amount of subarachnoid hemorrhage within the interpeduncular cistern (arrow).

[SWI]) surrounded by T2 hyperintense edema (Fig. 21). Blood products may have regions of diffusion restriction.

Diffuse Axonal Injury

In the setting of rotational acceleration and deceleration injuries, stretching or shearing injuries may occur within the axonal white matter, which is referred to as diffuse axonal injury (DAI). Due to the mechanism of injury, DAI is classified based upon the location of injury with higher grade injuries portending worsened neurological deficits and prognosis. Often times patients with DAI experience loss of consciousness at the time of injury and later display neurological deficits beyond what would be expected based upon the initial injuries identified on CT. Grade I injuries occur within the lobar white matter near the gray-white matter junction. Grade II injuries include the lobar white matter plus involvement of the corpus callosum with preferential involvement of the body and splenium of the corpus callosum. Grade III injuries involve the lobar white matter and corpus callosum with additional

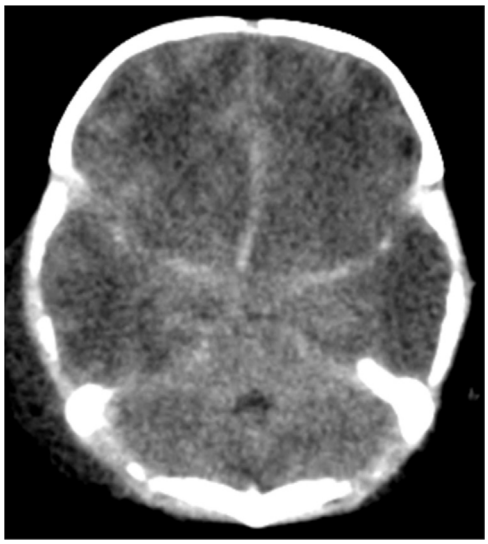

Figure 18 Pseudosubarachnoid hemorrhage in an infant with diffuse hypoxic-ischemic injury post-trauma. Axial noncontrast CT image through the basal cisterns reveals extra-axial hyperdensity mimicking subarachnoid hemorrhage due to vascular engorgement, CSF effacement, and adjacent parenchymal hypodensity.

Figure 19 Cortical contusion on CT following a fall. Axial noncontrast CT image shows a large hyperdense cortical contusion involving the right middle frontal gyrus (*). Foci of subarachnoid hemorrhage are seen within several sulci (arrows). Scalp soft tissue swelling is identified over the right frontal impact site.

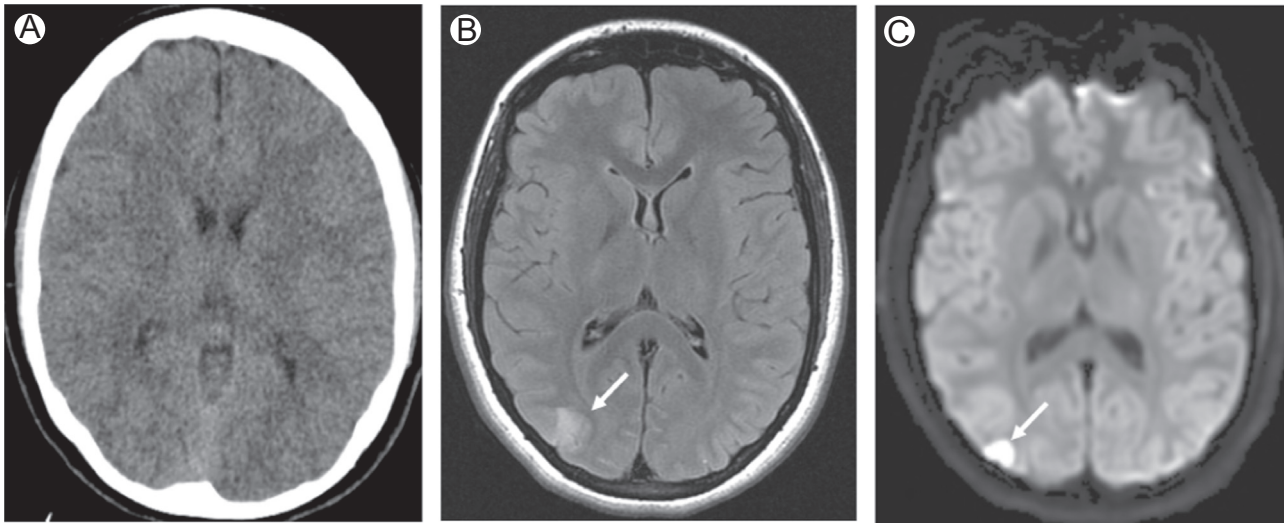

Figure 20 Cortical contusions better seen on MRI in a somnolent patient following closed head injury. Axial noncontrast CT image (A) demonstrates no focal parenchymal abnormality. On subsequent MRI examination performed a few hours later, there is a focal region of cortical and subcortical increased T2 FLAIR signal intensity (B) with restricted diffusion (C, ADC map not shown) involving the right occipital lobe (arrows).

involvement of the brainstem, often involving the rostral brainstem and superior cerebellar peduncles (Fig. 22).[15] Thalamic and basal ganglia involvement is also commonly associated with higher grade injuries.

On CT, DAI may be hemorrhagic or nonhemorrhagic. Hemorrhagic lesions are hyperdense and may have some surrounding edema (Fig. 23). Nonhemorrhagic lesions are hypodense on CT and can be subtle or even imperceptible, especially in infants with unmyelinated white matter. Lesions are typically multiple and can vary in size from a few millimeters to over a centimeter. The extent of injury, however, is typically underestimated on CT.[16]

MRI is more sensitive than CT in identifying regions of DAI. Hemorrhagic lesions demonstrate hypointense signal on T2* GRE or SWI with some adjacent edema. Nonhemorrhagic foci are typically T2 hyperintense. Some lesions may be best identified on diffusion weighted sequences, so it is important to carefully review all imaging sequences to identify areas with imaging manifestations of shear injury (Fig. 24).[17,18] Although not routinely performed, MR spectroscopy has been shown to

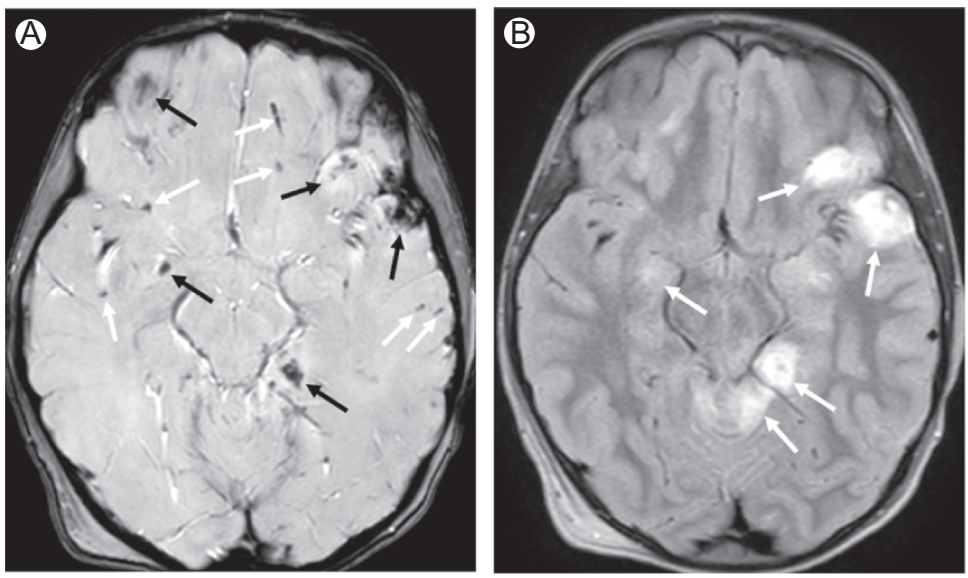

Figure 21 Hemorrhagic cortical contusions on MRI in a child hit by car while riding a bicycle. Axial susceptibility-weighed image (A) demonstrates multifocal regions of hypointensity/magnetic susceptibility involving the cortex and subcortical white matter of the left greater than right cerebral hemispheres (black arrows). Corresponding T2 FLAIR image (B) shows regions of edema surrounding the parenchymal contusions (white arrows) that are most pronounced within the left inferior frontal, anterior temporal, and posteromedial temporal lobes, as well as the superior cerebellum. Additional smaller contusions with magnetic susceptibility are seen within the right frontal and medial temporal lobes. Scattered subcortical white matter shear injuries are also visualized on susceptibility-weighted imaging (A, white arrows).

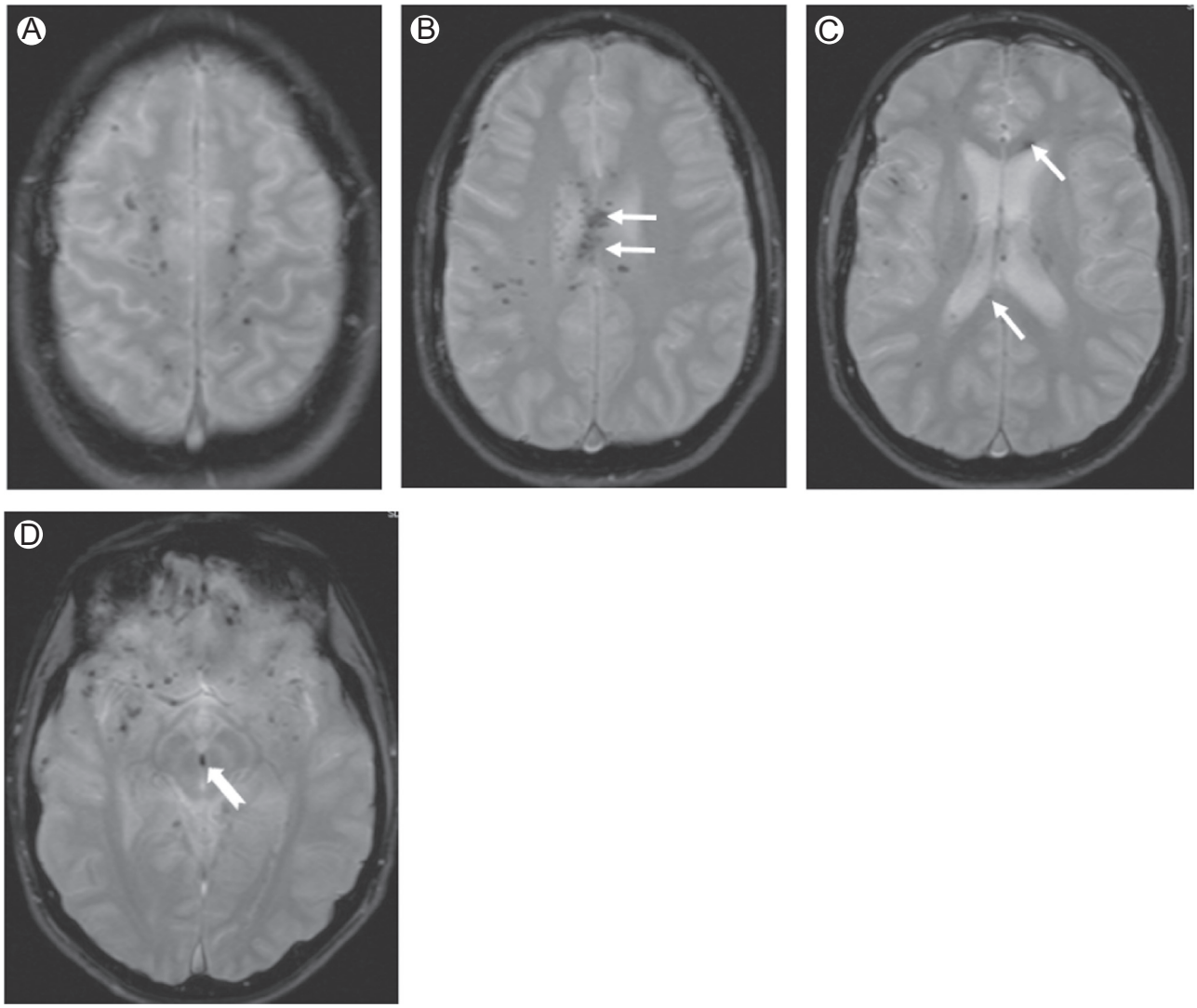

Figure 22 Patterns of diffuse axonal injury (DAI). Axial susceptibility-weighted images (A-D) show regions of hypointensity or magnetic susceptibility involving the subcortical white matter (A-D, grade 1), corpus callosum (B and C, arrows, grade 2), and brainstem or midbrain (D, notched arrow, grade 3). Image C also shows involvement of the superior portions of the basal ganglia and thalami.

identify regions of axonal injury that are not visualized on conventional MR sequences.[19]

Craniocervical Junction and Cervical Spine Injuries

Due to the large head size relative to a child's body, as well as undeveloped neck musculature, children—especially those under 8 years of age—are prone to injuries at the craniocervical junction and upper cervical spine in association with head trauma. For these reasons, it is important to include and closely review the craniocervical junction and portions of the cervical spine down to at least the C2 level on trauma head CTs. Although a detailed description of craniocervical and cervical spine injuries is beyond the scope of this review, common injuries include skull base fractures, atlanto-occipital dislocation, atlantoaxial instability, rotatory subluxation, and fractures and ligamentous injury of the upper cervical spine. Compared to adults, ligamentous injuries without associated fractures are more common in children. Therefore, in patients with neurological deficits despite the absence of fractures on cervical spine radiographs or CT, MRI should be obtained to look for ligamentous, cord, and soft tissue injuries.

Abusive Head Trauma

The role of imaging in the evaluation of suspected cases of abusive head trauma (AHT) is both important and complex. A comprehensive discussion of the neurological imaging manifestations of AHT is beyond the scope of this review; however, important and characteristic considerations will be discussed.

Head injury in association with AHT is unfortunately common and is a leading cause of morbidity and mortality in abused children. The pattern and extent of injury depend upon the underlying mechanisms and severity of trauma, which is often incompletely disclosed by caregivers. Common mechanisms of abusive head trauma include direct blows,

Figure 23 Hemorrhagic diffuse axonal injury on CT. Axial CT image demonstrates a left frontal subcortical region of hyperdense hemorrhage with minimal surrounding edema. An intracranial pressure monitor is partially visualized in the right frontal lobe.

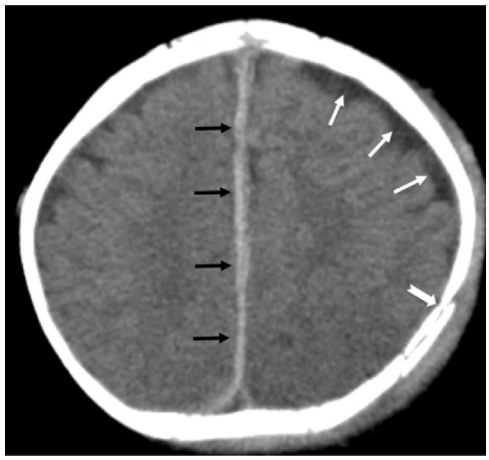

Figure 25 Subdural hemorrhage in an abused infant. Axial noncontrast CT image demonstrates hyperdense subdural hemorrhage within the interhemispheric fissure (black arrows). A small hypodense (isodense to CSF) subdural collection is seen overlying the left frontal lobe (white arrows). There is a left scalp hematoma with a nondisplaced left parietal bone fracture (notched arrow).

aggressive shaking, throwing or slamming down a child, suffocation, and strangulation.

With blunt trauma, calvarial injury and underlying intracranial hemorrhage are common. Subdural hematomas represent the most frequent pattern of intracranial hemorrhage in AHT (Fig. 25).[20] The CT appearance of an isolated subdural hematoma in abusive head injury may be identical to that previously described for accidental injuries. However, AHT should be considered when there are subdural hematomas, particularly with varying densities, and an injury pattern that is inconsistent with the clinical history provided. Internal septations or membranes located within the subdural collections imply chronicity associated with a more remote component (Fig. 26).[21,22] MRI is superior to CT in evaluating subdural hematomas due to the signal characteristics specific to the breakdown of blood products (Fig. 27). Aside from describing the attenuation and signal characteristics of blood products, one should be cautious in trying to date subdural hemorrhages. Extra-axial hemorrhages do not always follow predictable phases of evolution and the precise etiology for the observed signal characteristics can be multifactorial. Subarachnoid

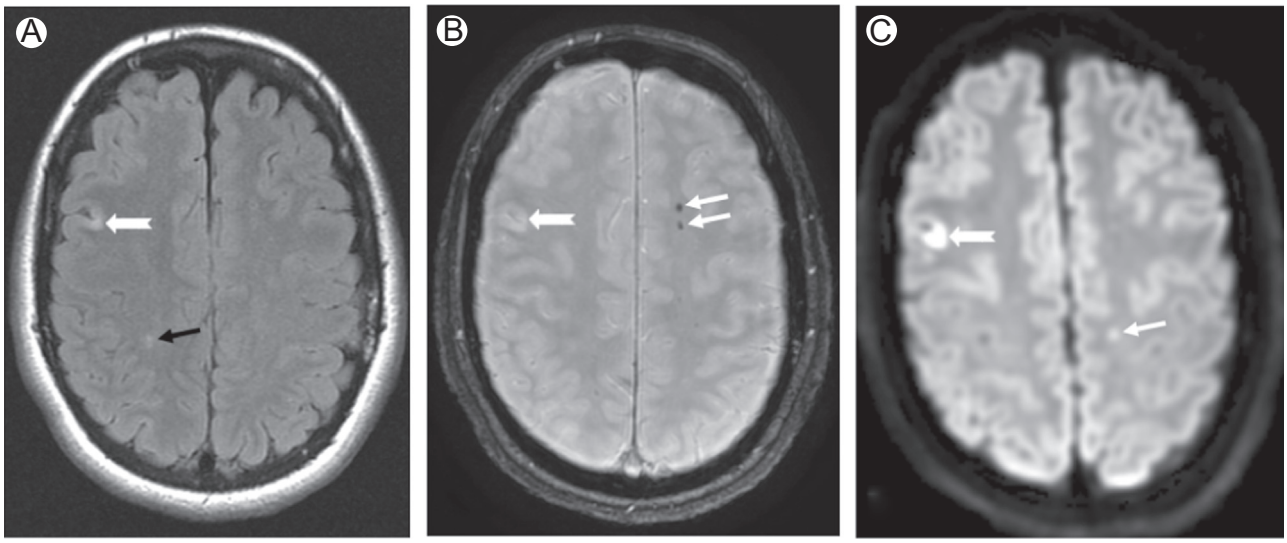

Figure 24 Visualization of DAI lesions on different MRI sequences. Axial T2 FLAIR (A), susceptibility-weighted (B), and diffusion weighted (C) images at the same level reveal an area of hyperintense signal involving the right frontal lobe (notched arrows), best visualized on the T2 FLAIR and DWI sequences. An additional focus of T2 FLAIR signal abnormality within the right parietal lobe white matter (A, black arrow) is not seen on SWI or DWI sequences. Small left frontal subcortical foci of hypointensity/magnetic susceptibility are seen on SWI (B, double white arrows), but not visualized on T2 FLAIR or DWI sequences. A small medial left parietal focus of hyperintense signal is seen on DWI (C, white arrow) but is not visualized on T2 FLAIR or SWI sequences.

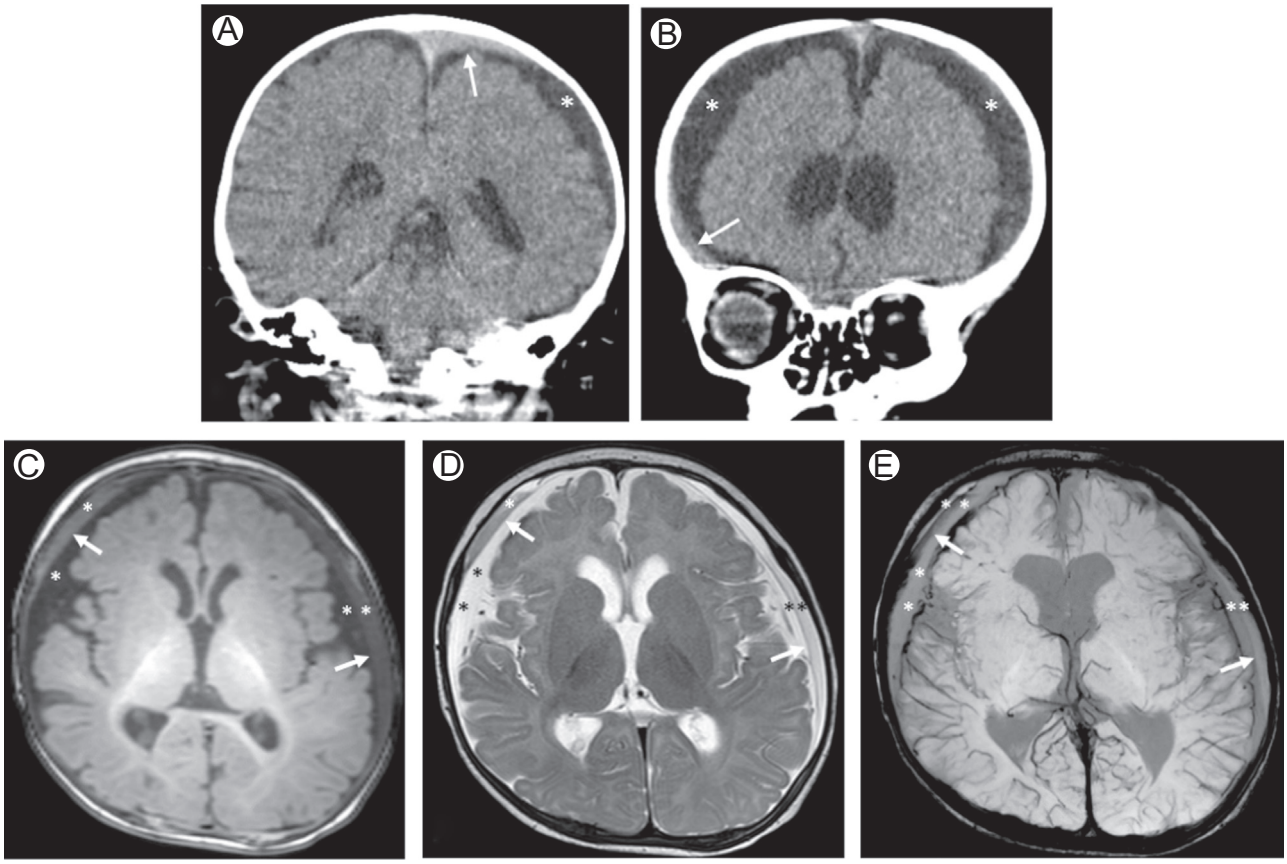

Figure 26 Subdural hemorrhages of differing densities or signal intensities with septations in the setting of AHT. Axial (A) and coronal reformatted (B) noncontrast CT images show bilateral predominantly hypodense subdural collections (*) with focal regions of hyperdense hemorrhage near the cranial vertex on the left and overlying the inferolateral right frontal lobe (white arrows). On follow-on MRI, there are mixed signal intensity subdural collections (*) with septations (arrows) on T1 (C) and T2 (D) weighted imaging. Susceptibility-weighted imaging (E) shows the subdural collections (*) with septations (arrows) and regions of magnetic susceptibility.

hemorrhage is the next most common pattern of intracranial hemorrhage in abusive head injury; when present, it is seen in association with subdural hemorrhages.

Calvarial fractures may be seen in the setting of both accidental and abusive head trauma with linear parietal bone fractures being most common in both patient populations. The presence of multiple fractures, stellate fractures, bilateral fractures, fractures that extend across sutures, and fractures without an appropriate history or mechanism are more commonly seen with AHT (Fig. 28).[23,24] Secondary findings

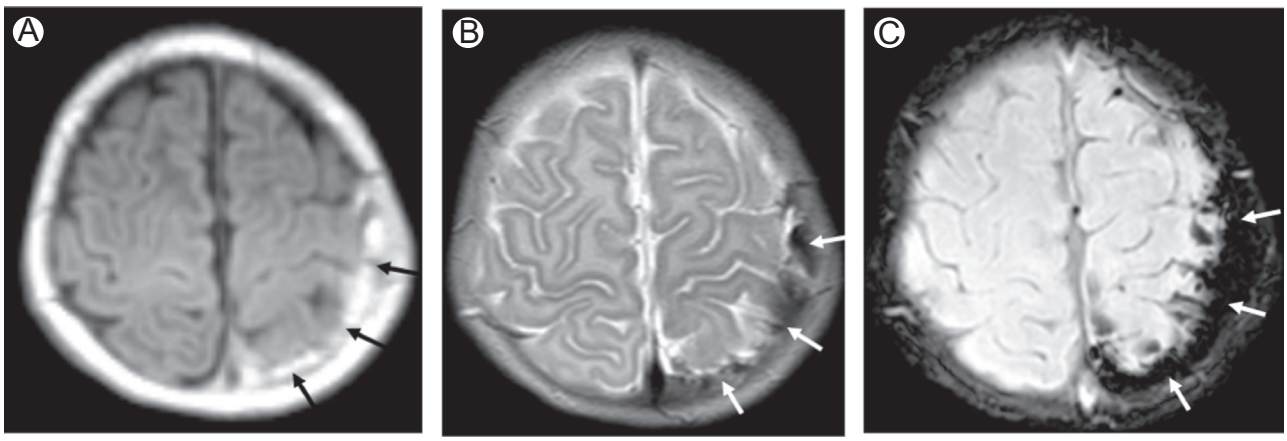

Figure 27 Evaluation of blood products on MRI in an abused infant. Axial T1 weighted MR image (A) shows a hyperintense subdural hemorrhage overlying the left parietal and posterior frontal lobes (black arrows). The subdural hemorrhage is hypointense on T2 (B) and susceptibility-weighted (C) imaging (white arrows) with blooming on susceptibility-weighted image.

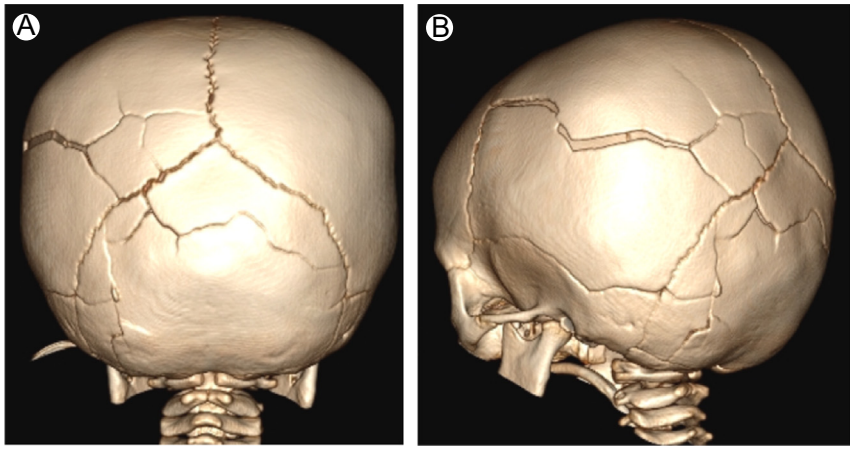

Figure 28 Complex, stellate calvarial fracture in an abused child. Posterior (A) and posterolateral oblique (B) volume rendered projections of the skull demonstrate a stellate fracture centered within the right posterior parietal bone near the lambdoid suture with multiple radiating fracture lines that cross sutures. (Color version of the figure available online.)

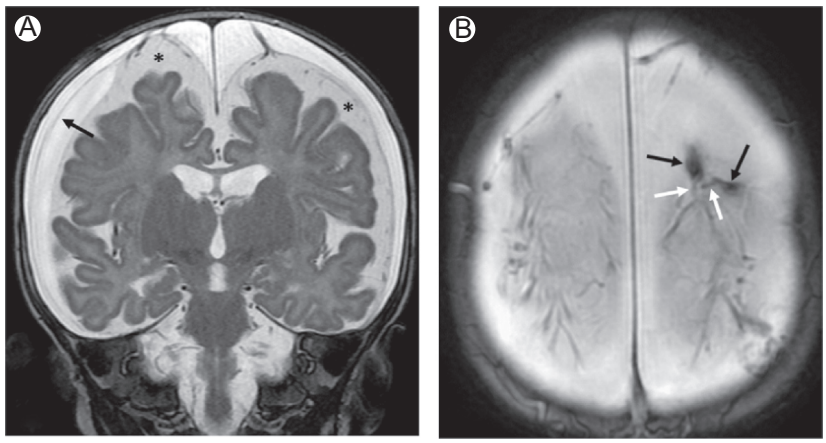

Figure 29 Cortical vein injury in an abused infant. Coronal T2 weighted image (A) shows bilateral subdural collections with a septation (arrow) on the right. There is prominence of the subarachnoid spaces (*) with diffuse parenchymal volume loss. Axial susceptibility-weighted image (B) demonstrates two "tadpole" signs with focal ovoid hypointense foci (body of tadpole, black arrows) and adjacent linear expanded bridging veins (tail of tadpole, white arrows) overlying the left cerebral hemisphere near the cranial vertex.

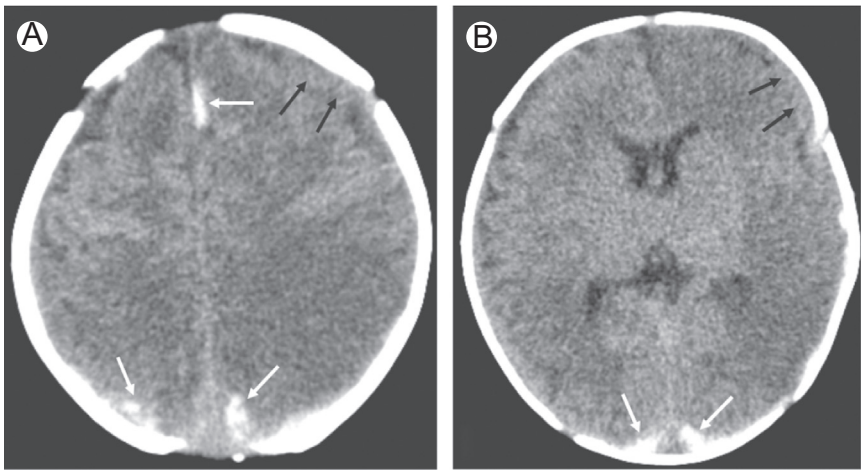

Figure 30 Hypoxic-ischemic injury in an abused infant. Axial noncontrast CT images (A and B) demonstrate diffuse loss of gray-white matter differentiation involving the left greater than right cortex and underlying white matter, with increased involvement in the watershed regions. Hyperdense subdural hemorrhage is seen within the interhemispheric fissure and overlying the posteromedial cerebral hemispheres (white arrows). An isodense subdural collection is seen overlying the left frontal lobe (black arrows).

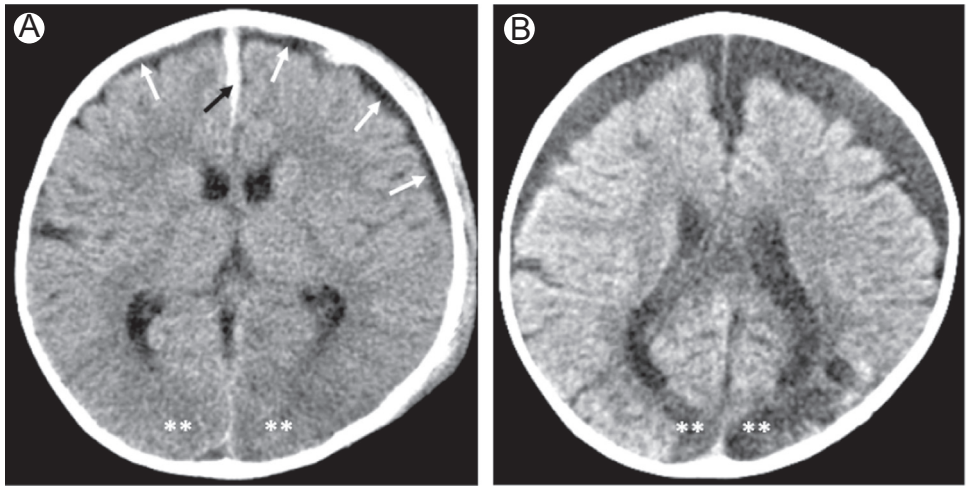

Figure 31 Sequela of hypoxic-ischemic injury in an abused child. Axial noncontrast head CT at the level of the deep gray matter nuclei (A) demonstrates a small left and tiny right predominantly hypodense subdural collections (white arrows), with hyperdense hemorrhage extending into the interhemispheric fissure (black arrow). There is loss of gray-white matter differentiation involving the occipital lobes (**). Follow-up noncontrast head CT at the level of the lateral ventricles several months later (B) shows diffuse parenchymal volume loss with occipital lobe encephalomalacia, left great than right (**). There are moderate-sized bilateral hypodense subdural collections.

of associated soft tissue swelling may or may not be present, even in the acute setting. With a delayed presentation, these secondary findings have typically resolved by the time of imaging.

"Shaken baby syndrome" refers to the mechanism of injury where a child is shaken vigorously in the anterior-posterior plane. With this mechanism, the brain parenchyma and calvarium move at different rates of acceleration and deceleration, which when combined with relatively large subarachnoid spaces, predisposes the child to tearing of bridging veins with resultant subdural hemorrhage. Retinal hemorrhages are commonly seen clinically. The presence of superficial bridging vein injury or thrombosis in the absence of an appropriate trauma history has been shown to be a positive indicator of AHT. Bridging vein injury is best depicted on susceptibility-weighted imaging and commonly results in the "tadpole" sign, as demonstrated by a focal round clot caused by bridging vein disruption (body of the tadpole) with an expanded thrombosed bridging vein (tail of the tadpole) (Fig. 29).[25] With severe trauma, hypoxic-ischemic injury (HII) may be seen in association with extra-axial hemorrhage and is more common in the setting of AHT compared to accidental injuries (Figs. 30 and 31). Common imaging patterns of HII include diffuse ischemic injury, watershed distribution injury, and, less commonly, focal injury or venous infarction.[26] Often the amount of subdural hemorrhage is small in relation to the extent of HII, but may serve as a potential marker of trauma. Despite the mechanism of injury in this population, diffuse axonal injury is relatively uncommon in AHT. Injuries to the craniocervical junction and cervical spine may also be seen due to the relatively large head size, orientation of facets, and underdeveloped musculature in children (Fig. 32).[23] Extracranial injuries with a high specificity for AHT include classic metaphyseal lesions and posterior rib fractures.[27]

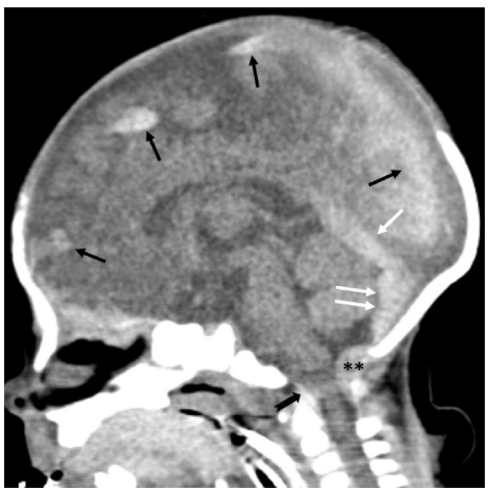

Figure 32 Craniocervical junction injury in an abused infant. Midline sagittal reformatted CT image demonstrates hyperdense subdural hemorrhage within the interhemispheric fissure (black arrows), along the tentorium (white arrow), and posterior to the cerebellar vermis (double white arrow). At the craniocervical junction, there is a small amount of hemorrhage along the posterior margin of the dens (notched black arrow) and a large extra-axial hemorrhage posteriorly (**), resulting in effacement of CSF at the foramen magnum.

Suffocation results in cerebral edema that is proportional to the severity and duration of the injury. Strangulation results in similar intracranial findings and may also result in vascular injuries that further exasperate the degree of intracranial edema.

Birth-Related Injuries

Intracranial Injuries

Birth-related injuries refer to those encountered during delivery and are more common with vaginal deliveries compared to cesarean section. Imaging of birth-related head trauma typically begins with ultrasound (US), followed by CT, if necessary.

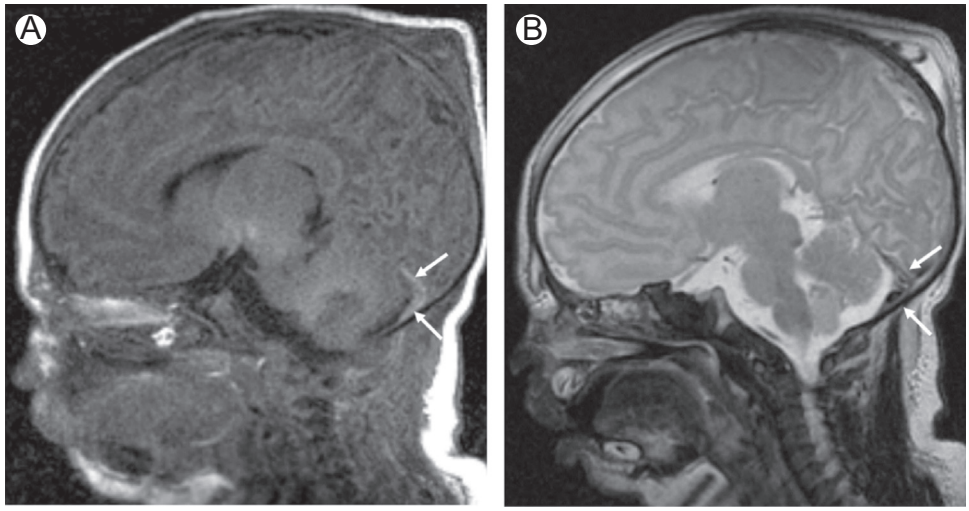

Figure 33 Birth-related subdural hemorrhage. Sagittal T1 (A) and T2 (B) weighted images in a newborn demonstrate a small amount of T1 hyperintense and T2 hypointense subdural hemorrhage at the junction of the falx and tentorium and extending inferiorly within the posterior fossa along the occiput (arrows). A scalp hematoma is also noted at the cranial vertex.

Although MRI is more sensitive in identification of hemorrhagic lesions not well seen on CT, the availability and speed of CT is preferred in the acute setting when US evaluation alone is insufficient.

In the normal birthing process, subdural hematomas are commonly seen, typically small, and of no clinical significance.[28,29] Although they may occur anywhere, including the posterior fossa, they most often occur at the junction of the falx cerebri and tentorium cerebelli (Fig. 33). Most are not well seen on US and are better characterized on CT or MRI. Beyond the acute setting, MRI not only has increased sensitivity for hemorrhagic lesions, but can also identify traumatic and ischemic white matter injuries that are not well visualized on CT.[30] Epidural and subarachnoid hemorrhage are less common in the setting of birth-related injuries, but when present, are often seen in association with subdural hematomas. Epidural hematomas have a higher incidence when associated with calvarial fractures and cephalohematomas,[31,32] often in the setting of a difficult birth requiring instrumentation.

Calvarial Fractures

As is seen with blunt head injury described previously, calvarial fractures may occur during a vaginal birth as the skull compresses against the mother's pelvis and undergoes remodeling or with the use of instrumentation (Fig. 34). Nondepressed fractures in this setting are of no clinical significance when seen in isolation and without secondary injuries.[33] Depressed fractures are less commonly seen but have a higher incidence of associated intracranial injuries.

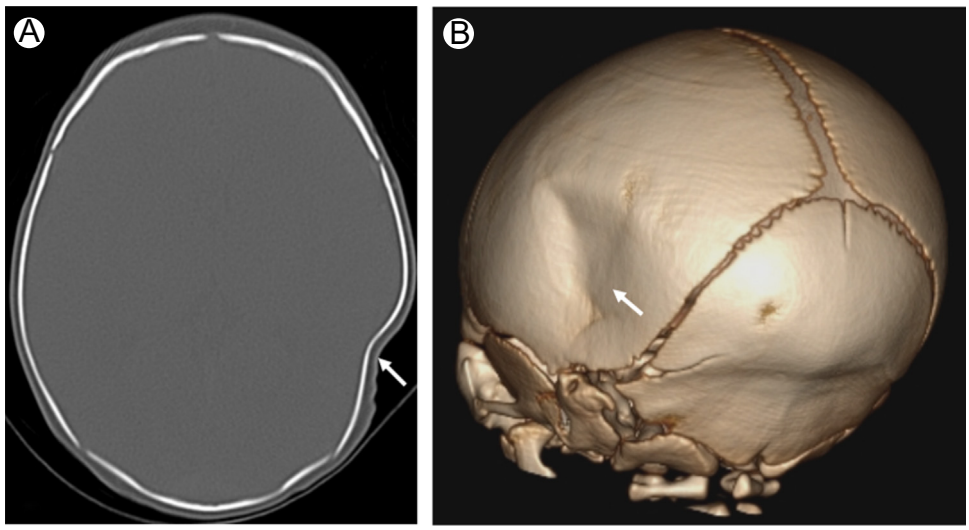

Figure 34 Birth-related calvarial remodeling or molding. Newborn after a prolonged and difficult vaginal delivery with the use of instrumentation (forceps). Axial CT image (A) shows inward depression of the left parietal bone (arrow). Volume rendered projection (B) better depicts the extent of calvarial depression (arrow) without an associated fracture lucency. (Color version of the figure available online.)

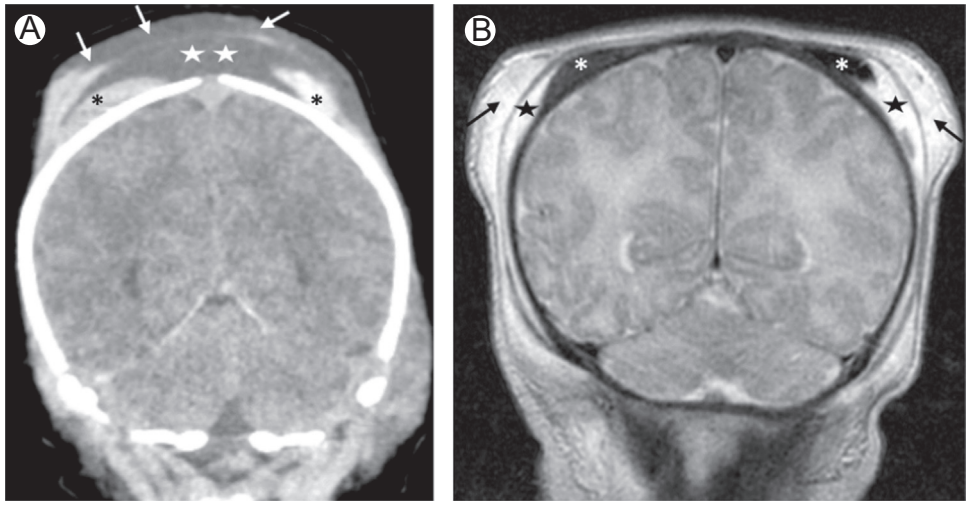

Figure 35 Birth-related scalp hemorrhage. Coronal reformatted CT (A) and T2 MR (B) images in a newborn child show hemorrhage and edema within all 3 compartments of the scalp. The cephalohematoma is subperiosteal in location and is hyperdense on CT and hypointense on T2 (*); it does not cross the sagittal suture. The subgaleal hemorrhage is located between the superficial subgaleal aponeurosis and the subjacent periosteum; it is hypodense on CT and hyperintense on T2 (5-point stars) and crosses midline. The caput succedaneum is superficial to the galeal aponeurosis and is mixed hyper and hypodense on CT and hyperintense on T2 (arrows); it crosses midline.

Extracranial Injuries

In addition to simple scalp hematomas, there are 3 primary types of superficial extracranial hemorrhage: caput succedaneum, subgaleal hemorrhage, and cephalohematoma. The distinction between the types of hemorrhage is based upon the compartment in which the hemorrhage occurs (Fig. 35).

Caput succedaneum refers to scalp hemorrhage superficial to the galeal aponeurosis (Fig. 35). It may spread throughout the scalp and cross midline since it is not bounded by periosteum or an aponeurosis. Most cases are self-limited.

A subgaleal hemorrhage occurs between the periosteum and overlying galeal aponeurosis, can also cross the midline and may extend into the soft tissues of the neck when large (Fig. 35). It most often results from instrumentation during a difficult birth with rupture of emissary veins. Although most cases are self-limited and resolve within a few weeks, large hemorrhages may be extensive and symptomatic.

A cephalohematoma refers to a subperiosteal hemorrhage that occurs between the underlying calvarium and overlying periosteum (Fig. 35). There is an increased incidence with prolonged labor and utilization of instrumentation. As the hemorrhage is subperiosteal in location, the hemorrhage is confined by sutures (cannot cross midline sagittal suture at cranial vertex) and is often firm. The hemorrhage can persist for months and rarely may calcify, forming a persistent calvarial contour abnormality (Fig. 36).[34]

Summary

Cross-sectional imaging plays an integral role in identifying and characterizing pediatric head trauma, which remains an important cause of morbidity and mortality in children. Understanding the patterns and appearances of head injury

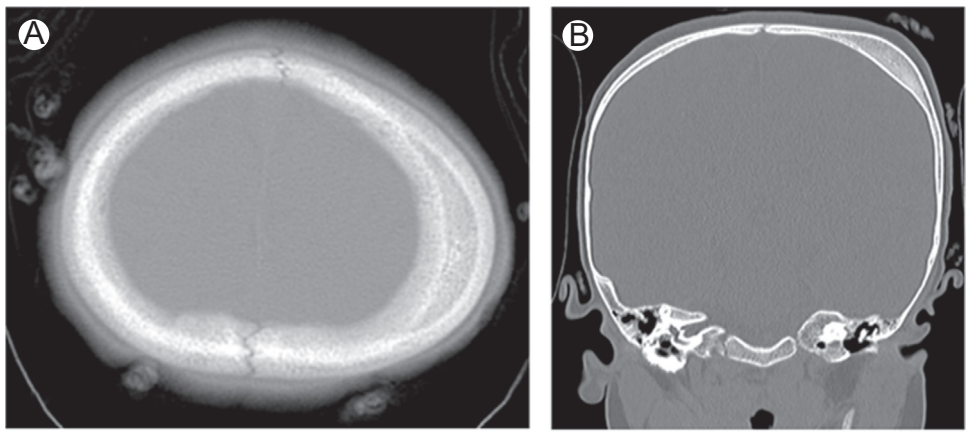

Figure 36 Calcified cephalohematoma. Patient with known prior birth-related scalp hematoma and persistent calvarial contour deformity. Axial (A) and coronal reformatted (B) CT images show a focal region of cortical thickening involving the superior portion of the left parietal bone, consistent with a calcified cephalohematoma.

on imaging studies and how they differ in children compared to adults is essential to the imaging evaluation. The key differences in children stem from the complexities of the developing brain and calvarium, as well as some unique mechanisms of injury, to include abusive head trauma and birth-related injuries. Knowledge of the intricacies of pediatric head trauma will assist the radiologist in appropriately evaluating the full spectrum of injuries and help guide appropriate patient management and follow-up.

References

1. American College of Radiology Appropriateness Criteria American College of Radiology Appropriateness Criteria; for head trauma in children for head trauma in children, 2014. https://acsearch.acr.org/docs/3083021/Narrative/. Accessed September 20, 2017.
2. PECARN Kuppermann N, Holmes JF, Dayan PS, et al: Identification of children at very low risk of clinically important brain injuries after head trauma: A prospective cohort study. Lancet 374(9696):1160-1170, 2009
3. Weir P, Suttner NJ, Flynn P, McAuley D: Normal skull suture variant mimicking intentional injury. Br Med J 332(7548):1020-1021, 2006
4. Sanchez T, Stewart D, Walvick M, et al: Skull fracture vs. accessory sutures: How can we tell the difference? Emerg Radiol 17(5):413-418, 2010
5. Idriz S, Patel J, Renani SA, et al: CT of normal developmental and variant anatomy of the pediatric skull: Distinguishing trauma from normality. RadioGraphics 35(5):1585-1601, 2015
6. Zergham Z, Morris AM, Paw R: Ping-pong fracture. Emerg Med J 24 (10):731, 2007
7. Liu XS, You C, Lu M, et al: Growing skull fracture stages and treatment strategy. J Neurosurg Pediatr 9(6):670-675, 2012
8. Parizel PM, Makkat S, Van Miert E, et al: Intracranial hemorrhage: Principles of CT and MRI interpretation. Eur Radiol 11(9):1170-1183, 2001
9. Al-Nakshabandi NA: The swirl sign. Radiology 218(2):433, 2001
10. Strub WM, Leach JL, Tomsick T, et al: Overnight preliminary head CT interpretations by residents: Locations of misidentified intracranial hemorrhage. Am J Neuroradiol 28(9):1679-1682, 2007
11. Given CA, Burdette JH, Elster AD, et al: Pseudo-subarachnoid hemorrhage: A potential imaging pitfall associated with diffuse cerebral edema. Am J Neuroradiol 24(2):254-256, 2003
12. Woodcock RJ, Davis PC, Hopkins KL: Imaging of head trauma in infancy and childhood. Semin Ultrasound CT MR 22(2):162-182, 2001
13. Poussaint TY, Moeller KK: Imaging of pediatric head trauma. Neuroimaging Clin N Am 12(2):271-294, 2002
14. Gentry LR: Imaging of closed head injury. Radiology 191(1):1-17, 1994
15. Adams JH, Doyle D, Ford I, et al: Diffuse axonal injury in head injury: Definition, diagnosis and grading. Histopathology 15(1):49-59, 1989
16. Mittl RL, Grossman RI, Hiehle JF, et al: Prevalence of MR evidence of diffuse axonal injury in patients with mild head injury and normal head CT findings. Am J Neuroradiol 15(8):1583-1589, 1994
17. Tong KA, Ashwal S, Holshouser BA, et al: Hemorrhagic shearing lesions in children and adolescents with posttraumatic diffuse axonal injury: Improved detection and initial results. Radiology 227(2):332-339, 2003
18. Hergan K, Schaefer PW, Sorensen AG, et al: Diffusion-weighted MRI in diffuse axonal injury of the brain. Eur Radiol 12(10):2536-2541, 2002
19. Holshouser BA, Tong KA, Ashwal S: Proton MR spectroscopic imaging depicts diffuse axonal injury in children with traumatic brain injury. AJNR Am J Neuroradiol 26(5):1276-1285, 2005
20. Barnes PD, Robson CD: CT findings in hyperacute nonaccidental brain injury. Pediatr Radiol 30(2):74-81, 2000
21. Hedlund GL: Subdural hemorrhage in abusive head trauma: Imaging challenges and controversies. J Am Osteopath Coll Radiol 1(1):23-30, 2012
22. Cramer JA, Rassner UA, Hedlund GL: Limitations of T2*-gradient recalled-echo and susceptibility-weighted imaging in characterizing chronic subdural hemorrhage in infant survivors of abusive head trauma. Am J Neuroradiol 37(9):1752-1756, 2016
23. Hsieh KLC, Zimmerman RA, Kao HW, et al: Revisiting neuroimaging of abusive head trauma in infants and young children. Am J Roentgenol 204(5):944-952, 2015
24. Meservy CJ, Towbin R, McLaurin RL, et al: Radiographic characteristics of skull fractures resulting from child abuse. AJR Am J Roentgenol 149(1): 173-175, 1987
25. Hahnemann ML, Kinner S, Schweiger B, et al: Imaging of bridging vein thrombosis in infants with abusive head trauma: the "Tadpole Sign." Eur Radiol 25(2):299-305, 2015
26. Zimmerman RA, Bilaniuk LT, Farina L: Non-accidental brain trauma in infants: diffusion imaging, contributions to understanding the injury process. J Neuroradiol 34(2):109-114, 2007
27. Lonergan G, Baker A, Morey M, et al: Child abuse: radiologic-pathologic correlation. RadioGraphics 23(4):811-845, 2003
28. Rooks VJ, Eaton JP, Ruess L, et al: Prevalence and evolution of intracranial hemorrhage in asymptomatic term infants. Am J Neuroradiol 29(6): 1082-1089, 2008
29. Tavani F, Zimmerman R, Clancy R, et al: Incidental intracranial hemorrhage after uncomplicated birth: MRI before and after neonatal heart surgery. Neuroradiology 45(4):253-258, 2003
30. Kelly AB, Zimmerman R, Snow RB, et al: Head trauma: comparison of MR and CT – experience in 100 patients. Am J Neuroradiol 9 (4):699-708, 1988
31. Choux M, Grisoli F, Peragut J: Extradural hematomas in children: 104 cases. Childs Brain 1(6):337-347, 1975
32. Tang HT, Lim CCT: Imaging of accidental paediatric head trauma. Pediatr Radiol 39(5):438-446, 2009
33. Rabelo NN, Matushita H, Cardeal DD: Traumatic brain lesions in newborns. Arq Neuropsiquiatr 75(3):180-188, 2017
34. Glass RBJ, Fernbach SK, Norton KI, et al: The infant skull: a vault of information. RadioGraphics 24(2):507-522, 2004